*Particle Accelerators*, 1994, Vol. 45, pp. 119–134
Reprints available directly from the publisher
Photocopying permitted by license only



# FOCUSING BEAMS WITH WIDELY VARYING CURRENT USING FIXED STRENGTH QUADRUPOLES FOR HEAVY-ION INERTIAL FUSION*

D.D.-M. HO,[1] K.R. CRANDALL[2] and I. HABER[3]

[1] *Lawrence Livermore National Laboratory, Livermore, CA 94550*

[2] *AccSys Technology, Inc., Pleasanton, CA 94588*

[3] *Naval Research Laboratory, Washington DC 20375*

*(Received 1 November 1993; in final form 2 March 1994)*

Ignition of an inertially confined thermonuclear pellet, driven by heavy-ion beams, requires nearly isentropic fuel compression and spark plug heating by shock waves. This implies that the power required for implosion, or the beam current (in the kiloampere range), must increase with time. At the same time, the beam must be focused onto a millimeter-size focal spot with essentially constant radius. Varying the fields of the final focusing magnets substantially to focus such a beam onto a fixed size spot is impractical because the field strength is high and the beam pulse is short. In this paper, we describe a method that, without changing the strengths of the magnets, can focus beams onto a sufficiently small focal spot while minimizing variation in spot radius over a large current range. This is achieved by realizing that if the emittance-generated pressure gradient is greater (smaller) than the beam space-charge force at the focal plane, the spot radius increases with decreasing (increasing) current. Thus, if the emittance generated pressure gradient is equal to the space-charge force at a current somewhere between the maximum and minimum beam currents, one can minimize the focal spot radius variation with changing current. Following this principle, final-focusing systems are designed using an envelope code. Particle-in-cell simulations verify that focal-spot radii are indeed insensitive to current change in these designs.

KEY WORDS: Accelerator Fusion, beam transport, heavy-ion accelerators, high-power beams

## 1 INTRODUCTION

Heavy-ion beam driven inertial confinement fusion (ICF) for commercial energy production is receiving increased attention[1] because of efficient beam-target[2] coupling and desirable features of heavy-ion accelerators, e.g., high repetition rate ($\gg$ 1 Hz),[3,4] high efficiency (up to 40%),[4] and good reliability over many pulses.

* Work performed under the auspices of the U.S. Department of Energy by the Lawrence Livermore National Laboratory under contract no. W-7405-Eng-48.

Ignition of an inertially confined thermonuclear pellet requires nearly isentropic fuel compression and spark plug heating by shock waves.[5,6] This implies that the power requirement for implosion, or the beam current (in the kiloampere range), must increase with time during the driving pulse [Figure 1(a)]. At the same time, the beam must be focused onto a millimeter-size focal spot with essentially constant radius. Unless attention is given to the design of the final focusing system, the focal-spot radius varies with the current, and a large fraction of the beam can fall outside the desired spot radius. This can severely degrade the energy gain of the fusion pellets.

Focusing beams with widely varying current onto a focal spot with fixed radius by pulsing the fields of the final-focusing magnetic quadrupoles is impractical because the field strength is high (several tesla) and the beam pulse is short (tens of nanoseconds). In this paper, we describe a new method (partially described in References 7, 8, and 9) that, without changing the quadrupole strengths, can still focus beams onto a focal spot with minimum variation in spot radius over a large range of beam current.

This method depends on the fact that the emittance is invariant along the beam (this turns out to be a reasonable assumption as we show later in this paper), despite the fact that the current is varying. Once the emittance is fixed, one can then adjust the beam parameters so that, for an intermediate current somewhere between the maximum and the minimum currents along the beam, the space-charge force equals the emittance-generated pressure gradient (which is the same as the thermal-pressure gradient) at the focal plane. Above this intermediate current, the space-charge force becomes dominant at the focal plane, and the focal-spot radius increases as the current increases. Below this intermediate current, the emittance-generated pressure gradient becomes dominant, and the focal-spot radius increases as the current decreases. This current and focal-spot radius relation results in a minimum in focal-spot radius as a function of current. Consequently, by designing the focusing system so that the minimum focal-spot radius falls somewhere near the center of the range of current to be focused, variation in spot radius over the total range of current can be substantially reduced. Note that even if the emittance varies along the beam, this method still works as long as the emittance variation is not too large.

Some implosions require that the current profile consist of a long initial pulse with constant current, followed by a shorter main pulse with a current five or six times higher than the initial pulse,[2] as shown in Figure 1(b). This current profile can easily be focused onto a fixed size spot by applying the above scheme. Also, as illustrated below, this scheme can be modified to reduce the spot-radius variation with current in the presence of chromatic aberration (caused by momentum spread). Vacuum chamber propagation is assumed in this paper.

Based on the above requirement, we have designed final-focusing systems using the envelope code TRACE.[10] We used the two-dimensional particle-in-cell (PIC) code SHIFTXY[11] to simulate the behavior of these systems. The simulation results verify that focal-spot radii are indeed insensitive to current variation in these designs.

The current and focal-spot radius relations shown in this paper are calculations based on parameters that are consistent with those used in the current heavy-ion fusion system studies. Actual accelerator design should provide enough flexibility for choosing

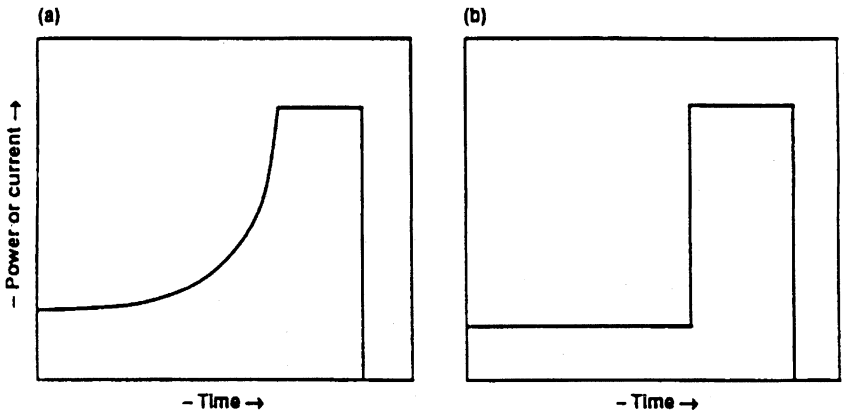


FIGURE 1: Generic power pulse requirement for ICF pellets: (a) smooth pulse with gradually increasing power; (b) stepped pulse.

the intermediate current needed for the scheme described here. For example, the required intermediate current can always be met by varying the number of beams while conserving the total beam power.

At the entrance of the final-focusing system, which in a typical heavy-ion fusion driver occurs after longitudinal beam compression, the beam must have the desired current variation along the beam as well as zero velocity tilt[12] in order to avoid chromatic aberration induced by the velocity tilt [the velocity tilt, in the beam-centered frame, is the head-to-tail velocity difference used for longitudinal beam compression]. Note that chromatic aberration can be caused by two sources: the intrinsic momentum spread and non-zero velocity tilt. Two-and-a-half dimensional (2-1/2-D) PIC simulations using CONDOR[13] demonstrate that it is feasible to compress a beam longitudinally such that the compressed beam satisfies the conditions required at the entrance of the focusing system.

In Section 2 of this paper, we describe the dependence of the focal-spot radius on beam current, emittance, and momentum spread and explain a scheme that can minimize the focal-spot variation with changing current. Section 3 presents designs of two final-focusing systems with and without momentum spread and the PIC simulations for these systems. Section 4 summarizes the results. The appendix presents the results from the PIC simulations, which show the feasibility of compressing a beam longitudinally, without increasing the emittance, so that the compressed configuration satisfies the conditions required at the entrance of the focusing system.

## 2 DEPENDENCE OF THE FOCAL-SPOT RADIUS ON BEAM CURRENT, EMITTANCE, AND MOMENTUM SPREAD

The dependence of the focal-spot radius on beam current, emittance, and momentum spread is discussed in this section, followed by a scheme that can minimize the variation of

focal-spot radius with current. To study this dependence, we assume two properties of the beam.

First, emittance is assumed invariant along the beam, even though the beam line-charge density $\lambda$ must increase from beam head to tail (Figure 1) in order to satisfy pellet compression requirement. This is a reasonable assumption because the beam $\lambda$ and emittance are uniform as it comes out of the source. As the beam traverses through the acceleration and the beam combining sections, the $\lambda$ remains roughly constant, the beam is long, and the velocity tilt is about a couple percent of the beam velocity. Therefore, even though the beam emittance may increase by one or two orders of magnitude from the time when the beam leaves the source until the beam reaches the final pulse compression section, the increase should be roughly uniform along the beam. As the beam enters the final pulse compression section, we first have to shape the beam $\lambda$ into a particular profile and then impose a velocity tilt so that the final compressed configuration can be obtained. These beam manipulations are assumed to be adiabatic and therefore the emittance should be conserved.[12] The 2-1/2-D Condor PIC simulation, presented in the appendix, confirms that these manipulations do not increase the emittance, and the emittance remains uniform (except near the beam ends) if the initial emittance at the entrance of the compression section is uniform.

Second, for parameter range of interest, the beam is space-charge dominated and hence the flow is nearly laminar and the density profile is essentially uniform, except perhaps near the focal plane, during traversal of the final-focusing system.[14] This is because the final focusing system is designed to avoid any small neck in the beam, except in the vicinity of the focal plane, as shown by an example in Sec. 3. The emittance term in the envelope description is not important as long as the beam envelope is large, i.e., a few times larger than the focal-spot radius for the beams with parameters used in this paper. Consequently, at the exit of the last quadrupole of the final-focusing system, both the radius $a_e$ of the circular beam envelope and the slope of this envelope $a_e'$ are proportional to $\sqrt{\lambda}$ (where the primed quantity is the derivative of that quantity with respect to the direction of beam propagation $z$).

With the above two properties of the beam as initial conditions for the beam entering the space between the last final-focusing magnet and the focal plane, we use the envelope code TRACE to calculate the spot size as a function of beam current for a beam with Kapchinsky-Vladimisky (K-V) distribution. For the moment, the beam particles are assumed to have uniform momentum along the beam. The consequence of momentum spread along the beam is discussed later in this section. The calculations presented in this section all start from the exit plane of the last quadrupole, and the distance L between that plane and the focal spot is 5 m. Figure 2 shows the schematic of the beam envelope.

Curve *aob* in Figure 3 shows the focal-spot size vs beam current for a 10-GeV beam with atomic weight 210, charge state 2, and unnormalized emittance $\varepsilon = 13.0$ mm·mrad at every point along the curve. At point $o$, near the bottom of the curve, the electrical current $I = 1.5$ kA and the focal-spot radius $r_f = 2.5$ mm. These parameters correspond to the condition that at the focal plane, the space-charge force equals the transverse pressure gradient due to the emittance $\varepsilon$. Hereafter, the current that satisfies this condition is referred to as "reference current $I_{\text{ref}}$". The space-charge force per unit mass is $6.39 \times 10^{-8} qI/A(\beta\lambda)^3 r_f$ in SI units, where $A$ is the beam atomic weight, $\beta\lambda$ is the usual relativistic factor, and $q$ is the charge

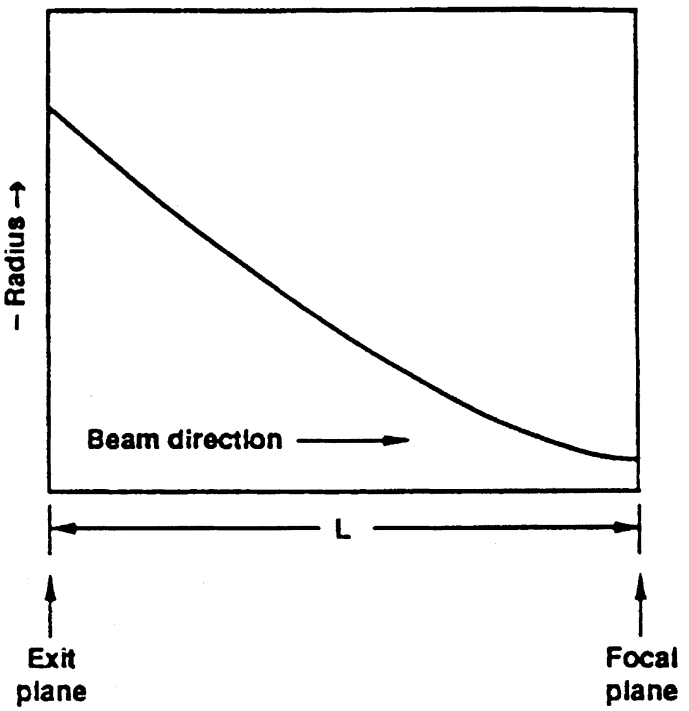


FIGURE 2: Schematic of the beam envelope between the focal plane and the exit plane of the last quadrupole.

state. The thermal-pressure gradient is $\varepsilon^2/r_f^3$. Equating these two forces and assuming $A$ = 210, particle energy to be 10 GeV, and thus $\beta\lambda = 0.323$, we obtain

$$qI_{\text{ref}}(kA) = 0.11\frac{\varepsilon^2\ (\text{mm}\cdot\text{mrad})}{r_f^2\ (\text{mm})}\ . \tag{1}$$

In this example, we have chosen the phase-space ellipse at the focal spot to be upright at point $o$.

To explain the fact that curve $aob$ has a minimum near point $o$, note that to the right of point $o$, the space-charge force exceeds the thermal-pressure gradient. At the limit when the emittance effect is negligible compared with the space-charge force, the flow is laminar, the density profile is uniform, and hence the envelope size is proportional to $\sqrt{\lambda}$ all the way to the focal spot. Consequently, focal-spot radius increases with current to the right of point $o$. Examination of the extreme right portion of curve $aob$ reveals that the focal-spot radius is indeed proportional to $\sqrt{\lambda}$ within a few percent.

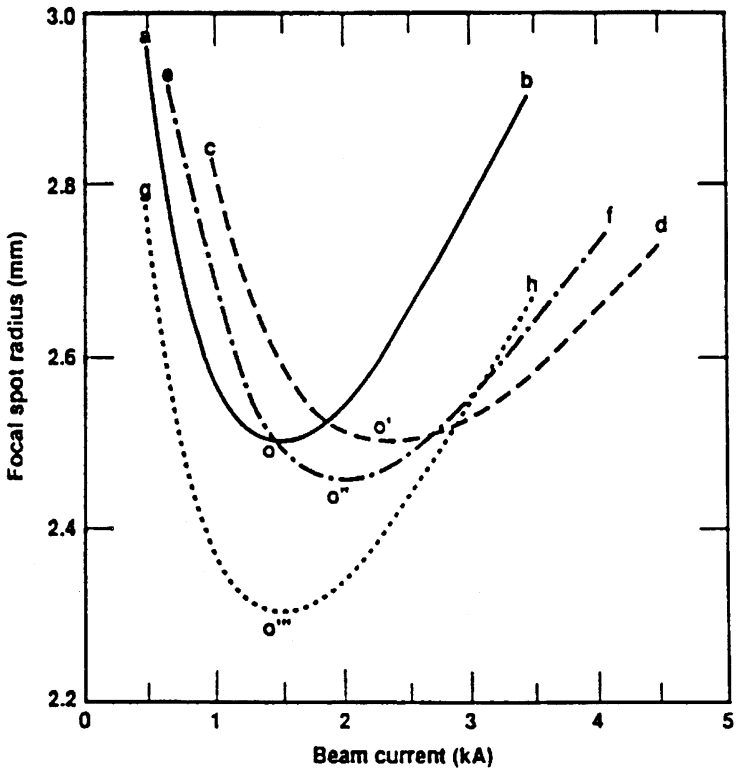


FIGURE 3: Focal spot radius vs beam current curves for free-space propagation: (a) curve *aob* — unnormalized emittance $\varepsilon = 13.0$ mm·mrad; (b) curve $co'd$ — $\varepsilon = 16.5$ mm·mrad; (c) curve $eo''f$ — $\varepsilon = 16.5$ mm·mrad (phase-space ellipse is not upright at point $o''$); (d) curve $go'''h$ — $\varepsilon = 12.0$ mm·mrad.

In the "low-current" regime, i.e., to the left of point $o$ (or $I_{\text{ref}}$) as the beam goes from large exit radius $a_e$ to final spot radius $r_f$, the importance of thermal-pressure gradient in determining the beam radius grows with respect to the space-charge term. As the beam current decreases further, the beam near the focal spot becomes emittance dominated. Under this condition, we can assume that particles move along straight-line orbits, so that the spot radius is given by

$$r_f = \frac{\varepsilon}{\theta}$$

where $\theta = a_e/L$ is the cone angle at the focal spot. Since the flow is laminar at the exit of the last magnet even though emittance can dominate in the vicinity of the spot, $a_e \propto \sqrt{\lambda}$ and consequently

$$r_f \propto \frac{1}{\sqrt{\lambda}}. \tag{2}$$

Hence, spot size increases as the current decreases to the left of point $o$. Examination of the extreme-left portion of curve $aob$ reveals that the focal-spot radius scales according to Equation (2) to within about 10%.

The above argument shows that minimizing the variation of focal-spot radius with current in the absence of momentum spread (or when the spread is corrected by sextupoles) requires positioning the minimum in spot radius somewhere between the maximum and the minimum beam currents. For example, for curve $aob$ shown in Figure 3, the current changes by a factor of 3 (from 0.8 to 2.65 kA), while the focal spot radius varies from 2.5 to 2.68 mm within this current range. If the desired radius is 2.6 mm, then the maximum and minimum radii differ from the desired radius by no more than 4%. Equation (2) shows that this method still works even if emittance varies along the beam, as long as the emittance variation $\varepsilon/\varepsilon_0$ is less than $\sqrt{\lambda/\lambda_0}$ where $\varepsilon_0$ and $\lambda_0$ are some reference values.

This example is for $\varepsilon$ = 13.0 mm·mrad. If the beam emittance has a different value, Equation (1) can be satisfied and the focal spot variation minimized at a different current. For example, when $\varepsilon$ = 16.5 mm·mrad and the beam atomic weight and velocity are the same as before, the reference current that satisfies Equation (1) is 2.4 kA. The focal-spot radius corresponding to this current is 2.5 mm and is point $o'$ on the focal-spot radius vs current curve $co'd$ shown in Figure 3. In this case, the current changes by a factor of 3 (from 1.35 to 4.05 kA), while the range of the focal-spot radius variation is from 2.5 to 2.65 mm. If the desired spot radius is 2.6 mm, then the maximum and minimum radii again differ from the desired radius by about 4%.

In the above examples, the phase-space ellipse at the focal spot is chosen to be upright at the reference current. This is, however, not a necessary condition for the scheme used to minimize the focal-spot variation described above. For example, if $\varepsilon$ = 16.5 mm·mrad and if we choose the phase-space ellipse to be upright with a radius of 2.5 mm at the focal spot at $I$ = 1.5 kA, then as the current increases, the focal-spot radius decreases until it reaches a minimum. At this minimum, the condition given by Equation (1) is approximately satisfied. This minimum spot radius is indicated as point $o''$ on curve $eo''f$ in Figure 3. As the current increases further, the spot radius begins to increase with current. Thus, one can equally well use curve $eo''f$ for minimizing focal-spot variation. To simplify the discussion in the rest of this paper, however, we choose the phase-space ellipse to be upright at the reference current.

For some implosion requirements, the current profile consists of a long initial pulse with constant current, followed by a short main pulse with current 5 or 6 times higher than the initial value, as shown in Figure 1(b). The scheme described above is readily applied to this case. For example, when $\varepsilon$ = 12.0 mm·mrad and the beam atomic weight is the same as before, the reference current that satisfies Equation (1) is 1.5 kA, with a focal-spot radius of 2.3 mm. This current corresponds to point $o'''$ on the focal-spot radius vs current curve $go'''h$, shown in Figure 3. On this curve, the focal spot has the same radius of 2.6 mm at about 0.625 and 3.25 kA. Thus, we can focus pulses with the shape shown in Figure 1(b) onto a fixed radius spot without varying the focusing magnetic field.

However, when the beam has a nonzero momentum spread, the above criterion must be modified because the increase in spot radius due to chromatic aberration also depends on current. When the relation between momentum spread and current is included, the beam should be in the low-current regime over the entire range of current because the spot

radius, without momentum spread, decreases with increasing current in this regime. This counteracts the increase in the spot radius with increasing current because the longitudinal temperature $T_z$ follows the 1-D adiabatic compression law,[12] i.e.,

$$T_z = T_z^0 \left(\frac{\lambda}{\lambda_0}\right)^2 , \tag{3}$$

where $T_z^0$ and $\lambda_0$ are the reference longitudinal temperature and line-charge density, respectively. Equation (3) shows that $T_z$, and hence chromatic aberration, increases with current. Thus, utilizing the cancellation of these two effects can minimize the variation of the spot radius. If the momentum spread is too large to be compensated by the emittance effect, then an alternative scheme for removing the chromatic aberration, e.g., the use of sextupoles, must be used.

The design of practical final-focusing systems, and PIC simulations verifying these designs, are presented in the following section.

## 3 FINAL-FOCUSING SYSTEM DESIGN AND PIC SIMULATIONS

This section presents two final-focusing systems designed to minimize the focal-spot radius variation with changing current, without and with chromatic aberration, and shows PIC simulations for these two systems.

We first present the design for the case without chromatic aberration, i.e., the design of a system that can produce the focal-spot radius vs current relation shown in Figure 3. Figure 4 shows the configuration of the focusing system that gives a 2.5 mm focal-spot radius with upright phase-space ellipse at $I_{\text{ref}}$ = 1.5 kA (point $o$ in Figure 3). In this figure, the beam is shown going through the last two periods of the magnetic quadrupole transport (FODO) channel. For this FODO channel, the value of $\sigma/\sigma_0$ [where $\sigma$ ($\sigma_0$) is the single-particle phase advance with (without) space charge] is 0.083 and the major and minor axes of the beam in the middle of a FODO magnet are 33.86 and 26.63 mm, respectively. This is followed by four magnets that change the beam into a waist (where the envelope has zero slope in both of the transverse directions), with the circular cross section having a 30.17-mm radius. The beam then undergoes free radial expansion due to space-charge forces and is focused by four final-focusing quadrupoles onto a 2.5 mm-radius focal spot. The beam envelope shown in Figure 4 is calculated using the envelope code TRACE. Table 1 lists the magnetic field gradients and the lengths of the quadrupoles.

Once the system has been designed for the reference current, the matched envelope size in the FODO transport channel is obtained for different currents. (The beam envelope remains matched along the beam, despite the fact that the current is varying, because the longitudinal pulse compression process is adiabatic.[12]) Using the matched beam as initial conditions, we then obtain the focal-spot sizes produced by this focusing system for different currents, as shown by curve *aob* in Figure 5. Curve *aob* is very close to the ideal focal-spot size

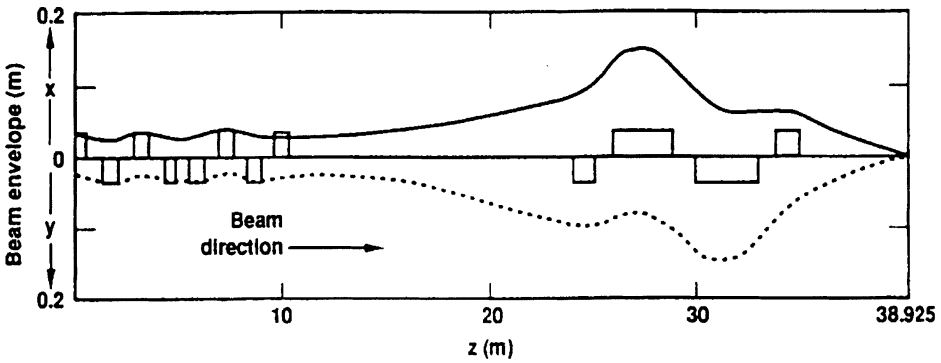


FIGURE 4: Final focusing system for charge-state-2, 10-GeV beam with atomic mass 210 and unnormalized emittance 13.0 mm·mrad. The upper and lower curves show the envelope in the $x$- and $y$-directions, respectively.

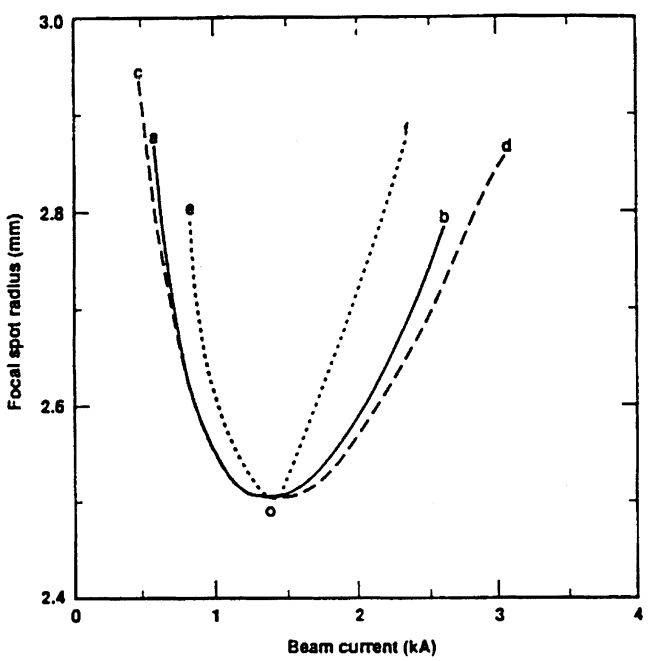


FIGURE 5: Focal-spot radius vs beam current: (a) curve *aob* — for the system shown in Figure 4; (b) curve *eof* — for the system shown in Figure 4, except the beam is being focused tighter (or having smaller transverse dimension) in the FODO channel; (c) curve *cod* — same as the curve *aob* shown in Figure 3.

TABLE 1: System parameters for a charge-state-2, 10-GeV beam with atomic mass 210 and unnormalized emittance 13 mm·mrad.

- Magnetic field gradients, lengths of the quadrupoles, and distance between the quadrupoles in the FODO transport system are ± 60.0 T/m, 0.75 m, and 0.75 m, respectively.
- Ratio of single-particle phase advance (degree per focusing period) with (current at 1.5 kA) and without space charge is 0.083.
- Parameters of the last four quadrupoles before the beam undergoes free-space expansion:

| Quadrupole number | Magnetic field gradient (T/m) | Quadrupole length (m) | Distance of quadrupole center to the waist (m) |
|---|---|---|---|
| Q1 | −30.70 | 0.825 | −4.6125 |
| Q2 | 70.82 | 0.800 | −3.1250 |
| Q3 | −59.48 | 0.825 | −1.7625 |
| Q4 | 23.29 | 0.725 | −0.5375 |

- Length of free-expansion region is 13.275 m.
- Parameters of the final focusing quadrupoles undergoes free-space expansion:

| Quadrupole number | Magnetic field gradient (T/m) | Quadrupole length (m) | Distance of quadrupole center to the waist (m) |
|---|---|---|---|
| Q5 | −18.65 | 1.075 | 13.8125 |
| Q6 | 15.84 | 2.700 | 16.6000 |
| Q7 | −17.43 | 2.700 | 20.3250 |
| Q8 | 25.12 | 1.150 | 23.1500 |

- Distance between the last focusing quadrupole and the focal spot is 5.0 m.

vs current curve, i.e., the curve *aob* shown in Figure 3 with $\varepsilon$ = 13.0 mm·mrad; this curve assumes laminar flow at the exit of the last quadrupole and is reproduced as curve *cod* in Figure 5. Therefore, this final focusing system accomplishes the goal of the design.

Note that in designing this system, the $\sigma/\sigma_0$ must be small, e.g., for the system shown in Figure 4, $\sigma/\sigma_0$ = 0.083 for $I$ = 1.5 kA. This means that the beam is strongly space-charge dominated. This condition allows the laminar flow condition at the exit of the last focusing quadrupole, as discussed in the previous section, to be satisfied and gives close agreement between curves *aob* and *cod* shown in Figure 5. In contrast, if $\sigma/\sigma_0$ is larger, e.g. $\sigma/\sigma_0$ = 0.124 for $I$ = 1.5 kA, then the laminar flow condition cannot be rigorously satisfied. Consequently, the focal spot radius is more sensitive to current variation, as shown by curve *eof* in Figure 5.

The discussions so far are based on the K-V distribution. To study the fraction of beam particles falling within a given focal spot radius with a more realistic initial distribution, e.g., semi-Gaussian (uniform in density and Gaussian in velocity), PIC simulations that include the self-consistent evolution of the beam distribution function have been performed. In the simulation using the PIC code SHIFTXY, automatic rezoning of the mesh as the beam

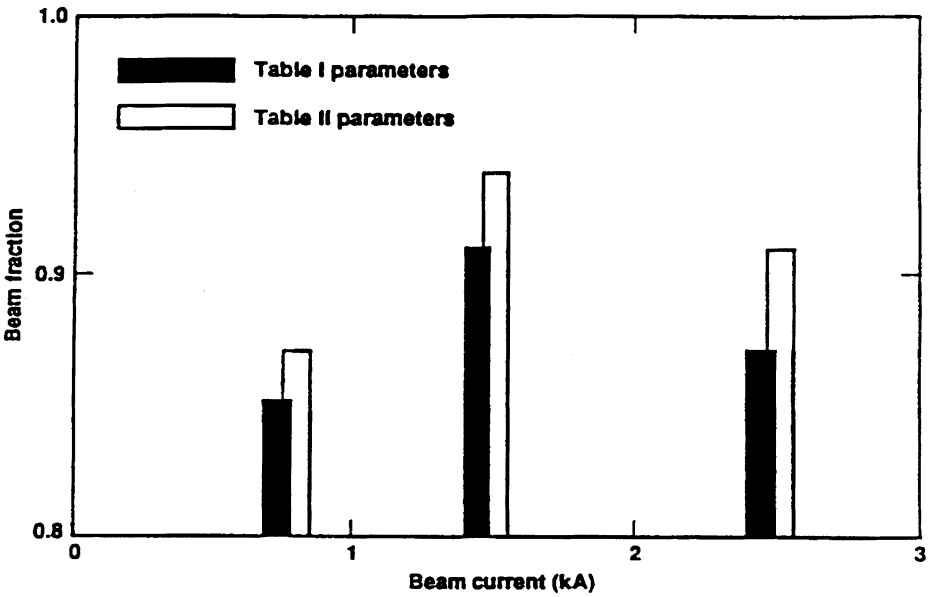


FIGURE 6: Fraction of beam on a 2.6-mm-radius spot for various beam currents focused by the systems with parameters given in Tables 1 and 2.

expands was used to minimize truncation errors in the numerical solution for the electric field. Using a 2.5-cm longitudinal step and a 256 × 256 mesh in a simulation with an initial K-V distribution to test the code, the rms radii generally agreed to within 1% of the envelope solutions up to the spot. As many as 64,000 particles were used to facilitate smooth diagnostics.

Figure 6 shows the results of simulations for the focusing system shown in Figure 4 performed with an initially semi-Gaussian distribution at 0.8, 1.5, and 2.5 kA. The black bars represent the fraction of beam particles falling within the desired focal-spot radius of 2.6 mm at those three currents. The fact that the variation of this fraction is only about 6%, while the beam current changes by a factor of 3, demonstrates the effectiveness of this scheme described in Section 2. Note that the fraction of beam particles falling within the K-V focal-spot radii obtained by TRACE is roughly constant at about 87 to 88%. These radii are 2.75, 2.5, and 2.68 mm at 0.75, 1.5, and 2.5 kA, respectively.

To minimize the spot-size variation for the case with nonzero momentum spread, the focal-spot radius vs current relation must be in the low-current regime, as discussed in the previous section. Also, the minimum focal-spot radius near the bottom of the focal-spot radius vs current relation must be less than 2.6 mm to accommodate the increase in spot radius due to chromatic aberration. The parameters for the final-focusing system, given in Table 2, provide such a focal-spot radius vs current relation, which is curve *ao* in Figure 7.

TABLE 2: System parameters for a charge-state-2, 10-GeV beam with atomic mass 210 and unnormalized emittance 15.14 mm·mrad.

- Magnetic field gradients, lengths of the quadrupoles, and distance between the quadrupoles in the FODO transport system are ± 60.0 T/m, 0.75 m, and 0.75 m, respectively.
- Ratio of single-particle phase advance (degree per focusing period) with (current at 3.0 kA) and without space charge is 0.05.
- Parameters of the last four quadrupoles before the beam undergoes free-space expansion:

| Quadrupole number | Magnetic field gradient (T/m) | Quadrupole length (m) | Distance of quadrupole center to the waist (m) |
|---|---|---|---|
| Q1 | −30.45 | 0.825 | −4.6125 |
| Q2 | 70.62 | 0.800 | −3.1250 |
| Q3 | −59.77 | 0.825 | −1.7625 |
| Q4 | 23.66 | 0.725 | −0.5375 |

- Length of free-expansion region is 13.275 m.
- Parameters of the final focusing quadrupoles:

| Quadrupole number | Magnetic field gradient (T/m) | Quadrupole length (m) | Distance of quadrupole center to the waist (m) |
|---|---|---|---|
| Q5 | −15.50 | 1.075 | 13.8125 |
| Q6 | 15.01 | 2.700 | 16.6000 |
| Q7 | −17.86 | 2.700 | 20.3250 |
| Q8 | 28.12 | 1.150 | 23.1500 |

- Distance between the last focusing quadrupole and the focal spot is 5.0 m.

The $I_{\text{ref}}$ for this curve is 3.0 kA. In this figure, the curve $bo'c$ is same as the curve $aob$ shown in Figure 5 with $\varepsilon$ = 13.0 mm·mrad, and is given for comparison.

The white bars in Figure 6 show the fraction of beam particles falling within a spot with 2.6 mm radius, in PIC simulations with momentum spreads $\Delta P/P_0 = 5.33 \times 10^{-4}$, $1.33 \times 10^{-3}$ and $1.67 \times 10^{-3}$ (where $P_0$ is the beam reference momentum and $\Delta P$ is the deviation from this momentum) at 0.8 kA, 1.5 kA, and 2.5 kA, respectively, and initial semi-Gaussian distribution. The distribution function is truncated at $3\sigma$ in the simulation. The variation of the beam fraction is only about 7%, while the beam current changes by a factor of 3.

## 4 CONCLUSION

A scheme has been presented for focusing beams with increasing current onto a focal spot with constant radius using fixed-strength quadrupoles. This is achieved by realizing that at low current, the thermal-pressure gradient dominates over space-charge force at the focal

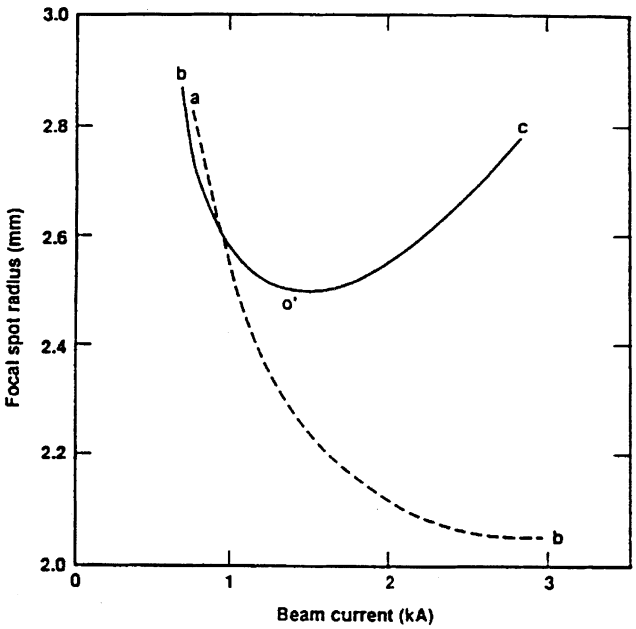


FIGURE 7: Focal-spot radius vs beam current: (a) curve *ao* — for the system with parameters given in Table 2; (b) curve *bo'c* — same as the curve *aob* shown in Figure 3.

plane, and the focal-spot radius increases with decreasing current. At high current, space-charge force dominates and the focal-spot radius increases with increasing current. The existence of a minimum in focal-spot radius as a function of current allows one to minimize the variation in focal-spot radius with changing current by choosing an intermediate current for which the thermal-pressure gradient equals the space-charge force at the focal plane. The minimum in focal-spot radius also allows a beam composed of two very different currents following one another to be focused onto a fixed radius spot. The effect of chromatic aberration on focal-spot radius can also be minimized by modifying this scheme. Simulations from PIC code with realistic particle distributions confirm the effectiveness of this scheme.

## ACKNOWLEDGEMENTS

We thank K. Hahn for discussion and are grateful to P. W. Murphy for editing the manuscript. Work performed under the auspices for the U.S. Department of Energy by the Lawrence Livermore National Laboratory under contract number W-7405-ENG-48, by AccSys Technology under SBIR contract number DE-AC03-89ER80768, and under the auspices of the Director, Office of Energy Research, U.S. Department of Energy

under contract number DE-AC03-76SF00098, Office of Basic Energy Sciences, Advanced Energy Project Division, through memorandum request number 4566410 from the Lawrence Berkeley Laboratory.

## APPENDIX : LONGITUDINAL COMPRESSION OF A UNIFORM BEAM INTO A CONFIGURATION WITH VARIABLE CURRENT AND UNIFORM VELOCITY

The longitudinal compression of an initially uniform beam to a higher uniform current and with no head-to-tail velocity variation is presented in Reference 12. By modifying this method, we show here that it is possible to compress a beam into a configuration with the nonuniform current profile desired for pellet compression and also no head-to-tail velocity variation. Simulation results, obtained from the CONDOR 2-1/2-D PIC code, are presented.

Figure 8 shows the variation with longitudinal coordinate of the initial line-charge density, radial distribution of beam particles, particle longitudinal velocity $v_z$, longitudinal temperature $T_z$, transverse temperature $T_\perp$, and normalized rms emittance in the $x$-direction. The initial beam is in radial force equilibrium with an imposed focusing electric field, which varies linearly with the radius [e.g., $E(r) = E_0 r$] and is independent of $z$. The method used to manipulate a uniform beam into the conditions shown in Figure 8, from a beam with initial parameters uniform in the longitudinal direction, is discussed in Reference 12. The beam shown in Figure 8 has a initial length of 4 m, maximum beam radius of 3 cm, maximum initial line-charge density of $1.2 \times 10^{-5}$ C/m, normalized rms emittance $2.95 \times 10^2$ mm·mrad, charge state 3, and atomic weight 210. Note that the longitudinal velocity increases toward the rear of the beam so that the beam will compress longitudinally.

The initial beam parameters specified above provide the initial conditions for a CONDOR PIC simulation. About $4 \times 10^4$ particles are used to simulate the self-compression. About 500 grid cells are used in the longitudinal direction, and the radial direction is divided into about 300 zones.

The initial radial electric field has the value $E_0 = -2.4 \times 10^8$ V/m and remains constant for the first $4.1 \times 10^{-7}$ s during the simulation. For the next $0.7 \times 10^{-7}$ s, this field is zero; then it rises to $-0.63 \times 10^8$ V/m. If the beam center is moving at $10^8$ m/s, this temporal variation of the radial electric field in the beam frame models the condition that the beam is being confined radially by a FODO system for a distance of 41 m, then undergoes free-space radial expansion for 7.0 m, and finally is confined radially again by the final focusing quadrupoles. (Transverse simulations have shown that the substitution of an azimuthally symmetric focusing force can be a good approximation to alternating gradient focusing.)

Under these conditions, the compression process is complete at about $5.4 \times 10^{-7}$ s; Figure 9 shows the desired beam configuration from the CONDOR simulation. Figure 9(a) shows that the $\lambda$ profile after compression is very close to the desired profile (dashed line); Figure 9(c) shows that the initial velocity tilt in the beam frame required for compression is removed by the force resulting from space-charge-generated longitudinal electric field. The emittance remains essentially invariant so that the transverse temperature approximately

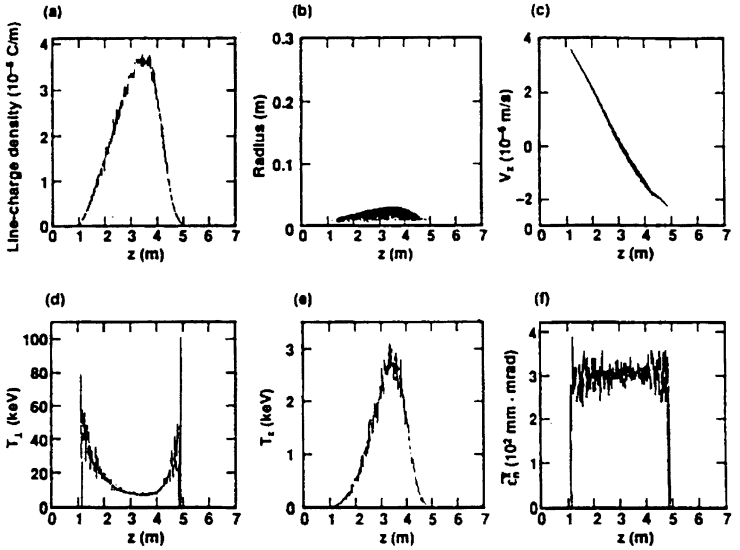


FIGURE 8: Beam initial parameters vs $z$: (a) line-charge density; (b) radial distribution of beam particles; (c) particle longitudinal velocities (in the beam frame); (d) transverse temperature; (e) longitudinal temperature; (f) normalized rms emittance in $x$-direction.

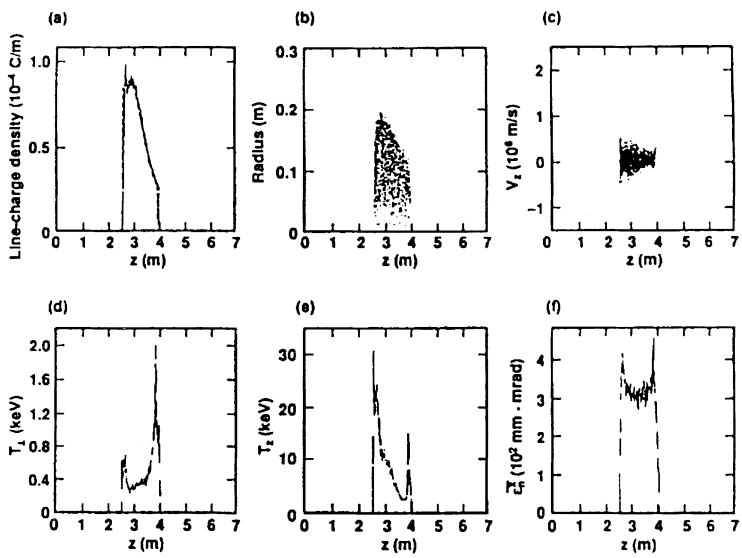


FIGURE 9: Beam parameters at the end of compression vs $z$: (a) line-charge density; (b) radial distribution of beam particles; (c) particle longitudinal velocities (in the beam frame); (d) transverse temperature; (e) longitudinal temperature; (f) normalized rms emittance in $x$-direction.

follows $T_\perp = T_\perp^0 (a_0/a)^2$ (where $T_\perp^0$ is the initial transverse temperature and $a_0$ is the initial beam radius),[12] and the beam radius is proportional to $\sqrt{\lambda}$ except at the beam ends, where emittance dominates. The longitudinal temperature approximately follows Equation (3).

The initial conditions, shown in Figure 8, are obtained by starting with the final conditions shown in Figure 9 as initial conditions, and performing the simulation with the time history of the radial electric field reversed. Since the compression is time reversible,[12] at $5.4 \times 10^{-7}$s, we obtain the $\lambda$ profile shown in Figure 8, except that the velocity tilt has opposite slope.

REFERENCES


1. C. Rubbia, "Inertial Fusion: A Contribution of Accelerator Technology to the energy Problem?" 3rd European Particle Accelerator Conf., Berlin (1992); T. J. Fessenden and A. Friedman, *Nuclear Fusion*, **31**, 1567 (1991).
2. D.D.-M. Ho, J.D. Lindl, and M. Tabak, "Radiation Converter Physics and a Method for Obtaining the Upper Limit for Gain in Heavy-Ion Inertial Fusion," accepted by *Nuclear Fusion*.
3. D.J. Dudjiak and W.B. Hermannsfeldt, "Heavy Ion Inertial Fusion," *Am. Inst. of Phys. Conf. Proc. 152*, M. Reiser, T. Godlove, and R.O. Bangerter, Eds., Washington, DC, p. 111 (1986).
4. J. Hovingh, V.O. Brady, A. Faltens, D. Keefe, and E.P. Lee, *Fusion Technology*, **13**, 255 (1988).
5. R.E. Kidder, *Nuclear Fusion*, **14**, 797 (1974).
6. R.E. Kidder, *Nuclear Fusion*, **19**, 223 (1979).
7. K.R. Crandall, Final Report to U.S. Dept. of Energy, contract No. DE-AC03-89ER80768 (1990); K.R. Crandall and D.D.-M. Ho, *Part. Accelerators*, **37–38**, 105 (1992).
8. D.D.-M. Ho, disclosure and record of invention No. IL-8227, Lawrence Livermore National Laboratory, Livermore, CA (1989); D.D.-M. Ho, *Bull. Am. Phys. Soc.*, **34**(9) 2172 (1989).
9. A.W. Maschke, private communication.
10. K.R. Crandall, Los Alamos National Laboratory, Los Alamos, NM, LA-11054-MS (1987).
11. I. Haber and H. Rudd, "Linear Accelerator and Beam Optics Code," *Am. Inst. of Phys. Conf. Proc. 177*, New York, NY (1988), p. 161; I. Haber, "High Current, High Brightness, and High Duty Factor Ion Injectors," *Am. Inst. of Phys. Conf. Proc. 189*, New York, NY, p. 107 (1986).
12. D.D.-M. Ho, S. T. Brandon, and E.P. Lee, *Part. Accelerators*, **35**, 15 (1991).
13. J.J. Ambrosiano, S.T. Brandon, D.E. Nielsen, and S. Ray, "A Brief Introduction to CONDOR," Lawrence Livermore National Laboratory, Livermore, CA, UCRL-ID-108037 (1991).
14. D.D.-M. Ho, I. Haber, K.R. Crandall, and S.T. Brandon, *Part. Accelerators*, **36**, 141 (1991).